

Observation of far-infrared emission from excited cytosine molecules

Y. C. Shen,^{a)} P. C. Upadhy,^{b)} and E. H. Linfield^{b),c)}

Cavendish Laboratory, University of Cambridge, Madingley Road, Cambridge CB3 0HE, United Kingdom

A. G. Davies

School of Electronic and Electrical Engineering, University of Leeds, Leeds LS2 9JT, United Kingdom

(Received 7 April 2005; accepted 19 May 2005; published online 29 June 2005)

We report a time-resolved investigation of the resonant absorption of far-infrared radiation and the subsequent vibrational relaxation processes in a sample of polycrystalline cytosine at 4 K, using terahertz time-domain spectroscopy. The subpicosecond time resolution achieved in our experiments corresponds to a near single-cycle of far-infrared radiation, and this enables us to observe the damped oscillations of the electric field produced by excited molecules as they decay. Furthermore, we show that the progressive absorption and subsequent emission of far-infrared radiation at the frequency of the corresponding vibrational mode can be followed directly as a function of time by means of time-partitioned Fourier transforms of the transmitted signal. © 2005 American Institute of Physics. [DOI: 10.1063/1.1968412]

According to the classical oscillator model of radiative transitions, when an energetically excited molecule returns to its ground state, a damped oscillating electric field is emitted with a characteristic resonance frequency and damping constant that is unique to each transition.¹ The direct observation of such a decaying oscillating electric field, however, requires experimental techniques with a temporal resolution better than the oscillating period. For transitions with characteristic energies corresponding to the visible and ultraviolet regions of the electromagnetic spectrum, the radiation frequency is too high to allow the direct measurement of this oscillating electric field.^{2–4} However, if the emission is in the far-infrared spectral range, a technique for measuring the electric field with a subpicosecond time resolution would allow this to be achieved. We demonstrate here the use of terahertz (THz) time-domain spectroscopy⁵ for such a study, investigating the time-resolved absorption and subsequent vibrational relaxation processes in molecules. Time-partitioned Fourier transforms of the measured THz time-domain signal reveal that an initial absorption of THz pulses is followed by the emission of THz radiation at the frequency of the corresponding vibrational mode.

Our experimental apparatus for coherent generation and detection of THz radiation⁶ is shown in Fig. 1. A Ti:sapphire laser provides optical (visible/near-IR) pulses of 12 fs duration at a center wavelength of 790 nm with a repetition rate of 76 MHz. The output is split into two parts. A 300 mW optical beam is focused onto the surface of a biased GaAs photoconductive emitter for generating near single-cycle THz pulses. The THz pulses generated are collimated and focused by a pair of parabolic mirrors onto the sample; the sample absorbs THz radiation and is pumped to an excited state. The transmitted THz pulse (together with the far-infrared radiation emitted from the excited molecules as they relax) is then collected by another pair of parabolic mirrors

and focused onto a 1 mm thick ZnTe electro-optic crystal, where it overlaps with a second optical beam (30 mW) that is used for electro-optic detection.⁷ A variable delay stage (with a 5 mm scan length) provides a time delay between the arrival of the THz pulse and the probing optical pulse at the electro-optic crystal, and allows the THz electric field to be mapped as a function of time. Fourier transforming the measured time-domain THz pulses gives the spectral response over a broad frequency range of 0.2–3.5 THz. A unique feature of time-domain THz spectroscopy is that the transient electric field itself is measured, not just the intensity of the THz radiation. Furthermore, the coherent detection scheme allows pulses to be measured below blackbody radiation levels with subpicosecond time resolution, corresponding to a near single-cycle of far-IR radiation ($33 \text{ cm}^{-1} \equiv 1 \text{ THz} \equiv 1 \text{ ps}$).⁵

Samples were prepared by mixing finely milled cytosine polycrystalline powder (Sigma-Aldrich, Lot 11K1313) with polyethylene powder (Sigma-Aldrich, Lot 17410AO-061) in a mass ratio of 1:10, and then compressing the mixture with

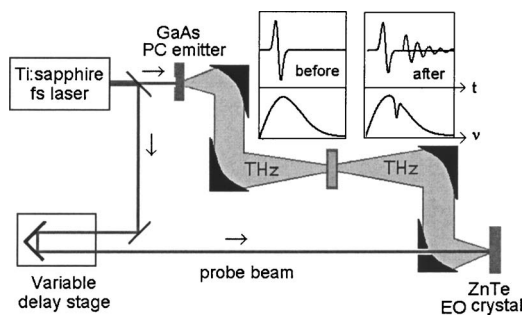


FIG. 1. Schematic representation of the experimental apparatus. Near single-cycle THz pulses are generated from a biased GaAs photoconductive (PC) emitter. The electric field of the transmitted THz pulse is then detected as a function of time using a 1 mm thick (110) ZnTe crystal via broadband electro-optic (EO) sampling. Inset: Schematic representation of the THz radiation before (left) and after (right) transmission through a sample. In the frequency domain, the absorption simply causes a spectral dip (bottom-right) at the resonance frequency of the sample. In the time domain, absorption is followed by subsequent radiation of a decaying electric field (solid curve, top right), in addition to the transmitted THz pulse (dashed curve, top right).

^{a)}Present address: TeraView Limited, Platinum Building, St John's Innovation Park, Cambridge CB4 0WS, UK.

^{b)}Present address: School of Electronic and Electrical Engineering, University of Leeds, Leeds LS2 9JT, UK.

^{c)}Author to whom correspondence should be addressed; electronic mail: e.h.linfield@leeds.ac.uk

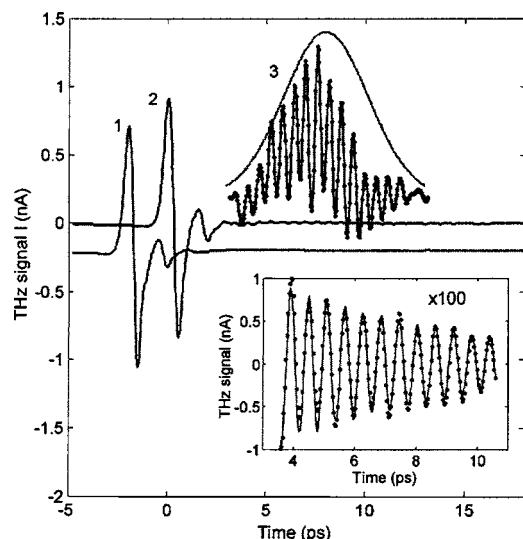


FIG. 2. THz pulse measured in the absence of a sample (curve 1) and after transmission through a polycrystalline cytosine sample at 4 K (curve 2). Fast oscillations are observed (in curve 2) immediately after the main peak (see inset). Curve 3 shows an amplified ($\times 100$) portion of curve 2 between 3 and 13 ps (dotted line) weighted by a 4 ps Gaussian window centred at 8 ps. All signals are vertically offset for clarity. Inset shows the measured (point) and calculated (line) THz signal between 3.5 and 10.5 ps.

a specially designed pellet maker to fit into a copper ring of 8 mm diameter. The pellet samples were about 1.3 mm thick. The copper ring ensures adequate thermal contact while allowing the THz beam to pass through the sample. The sample was fixed via the copper ring into the cold finger of a cryostat equipped with Mylar® windows, allowing THz spectroscopy measurements to be undertaken at 4 K. Note that polyethylene is nearly transparent in the frequency range 0.2–3.0 THz,⁸ and thus is a suitable filling material for spectroscopic applications in this spectral region.

Figure 2 shows the temporal electric field measured in the absence of a sample [$E_1^{\text{THz}}(t)$: curve 1] and after transmission through the cytosine sample [$E_2^{\text{THz}}(t)$: curve 2] at 4 K. Small, but pronounced, oscillations are visible immediately after the main pulse in curve 2 (Fig. 2 inset) that are not present in curve 1, indicating that they arise from the presence of the cytosine sample. One would expect the decaying electric field radiated by a molecule to be given by:¹ $E(t) = A \exp(-t/\tau) \sin(2\pi\nu t + \phi)$, where ν is the transition center frequency, τ is the decay constant of the transition, and A and ϕ are arbitrary constants. As shown in the inset of Fig. 2, good agreement between the fitted and measured data is obtained, with the best-fit value of the center frequency (ν) = 1.7 THz, and the decay constant (τ) = 6.5 ps. The decay constant corresponds to the lifetime of excited cytosine molecules, with such a short lifetime suggesting that there is strong intermolecular interaction in these samples even at a temperature as low as 4 K.¹

We calculated the transmission spectrum $T(\nu)$ by Fourier transforming and normalizing the time-domain THz signals:

$$T(\nu) = \frac{\int_{-\infty}^{\infty} E_2^{\text{THz}}(t) \exp(j2\pi\nu t) dt}{\int_{-\infty}^{\infty} E_1^{\text{THz}}(t) \exp(j2\pi\nu t) dt} \times \exp(j2\pi\nu t) dt.$$

This is shown in Fig. 3(a) (top curve), where a well-resolved spectral feature centered at 1.7 THz is observed. This spec-

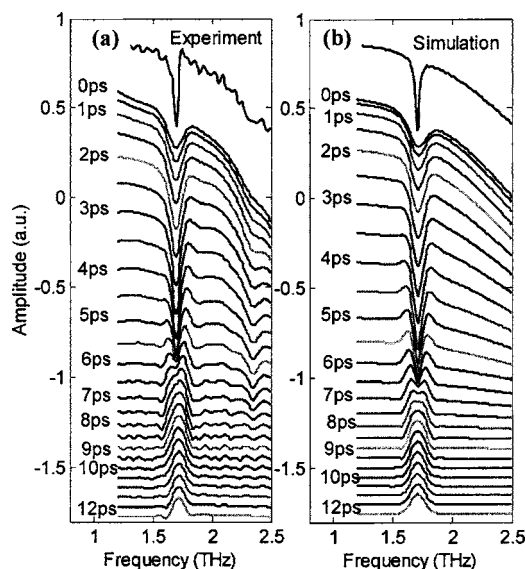


FIG. 3. (a) The time-partitioned Fourier transform spectra of the measured THz signals for cytosine at 4 K. The time interval between two adjacent curves is 0.5 ps, with the time on the left-hand side of the graph being the center of the 4 ps wide Gaussian window. The top curve is the transmission spectrum of cytosine. (b) The time-partitioned Fourier transform of the simulated THz data for a Lorenz oscillator ($\nu = 1.7$ THz, $\Gamma = 0.033$ THz, $S = 0.0005$). The time on the left-hand side of the graph is the center of the 4 ps wide Gaussian window. The top curve shows the simulated transmission spectrum.

tral feature corresponds to vibrational modes originating from intermolecular interactions mediated by hydrogen bonds.^{6,8} The small-amplitude, ripple-like oscillations in this spectrum results from multiple THz reflections in the sample and the detection crystal.

To study the time dependence of the absorption and emission by the cytosine sample, the time-partitioned Fourier transforms were next calculated in a confined Gaussian window:

$$T_i(\nu) = \frac{\int_{-\infty}^{\infty} E_2^{\text{THz}}(t) \exp[-(t-t_i)^2/(\Delta t)^2] \times \exp(j2\pi\nu t) dt}{\int_{-\infty}^{\infty} E_1^{\text{THz}}(t) \exp(j2\pi\nu t) dt},$$

where t_i ($t_i = 0, 0.5, 1.0, 1.5$ ps, ...) represents the center time of the Gaussian window of width Δt . Curve 3 of Fig. 2 shows such a Gaussian window ($\Delta t = 4$ ps), centered at 8 ps. By applying a Gaussian window to the measured THz waveform prior to performing the Fourier transform, we calculate the spectral response of the THz signal in a confined time period (for example, in Curve 3, 6–10 ps for a 4 ps wide Gaussian window, centered at 8 ps). This allows us to investigate the time-resolved absorption and subsequent vibrational relaxation processes. We note that the time resolution can be improved, at the expense of spectral resolution, by decreasing the width of the Gaussian window. For consistency we used $\Delta t = 4$ ps in all analyses.

Figure 3(a) shows a series of time-partitioned Fourier transforms calculated for successively later sampling windows after the main transmitted THz pulse; the time delay between the main transmitted THz pulse and the center of the Gaussian window is shown to the left of the spectra. At early times (0–4 ps after the incident THz pulse), spectra are

dominated by a dip at 1.7 THz resulting from resonant absorption by the cytosine molecules [see the transmission spectrum of cytosine in the top curve of Fig. 3(a)]. At later times (7–12 ps after the incident THz impulse), we observe a spectral peak, rather than a dip, suggesting that the resonant absorption of the THz pulse at 1.7 THz is subsequently followed by the emission of THz radiation at the same frequency as the vibrational mode. An intermediate state exists between 3 and 6 ps after arrival of the incident THz pulse.

We modeled the THz absorption and emission using a classical oscillator model.¹ The calculation was performed assuming that a specific molecular vibration can be described as a Lorentz oscillator (resonance frequency ν_0 , oscillator strength S , and relaxation time $1/\Gamma$), resulting in a characteristic absorption and refractive index profile described by: $\varepsilon(\nu) \equiv [n(\nu) + ik(\nu)]^2 = \varepsilon_r + S\nu_0^2 / (\nu_0^2 - \nu^2 - i\nu\Gamma)$. The transmitted THz signal was then calculated by taking into account the temporal shape of the incident THz pulse and multiple reflections in the sample. The time-partitioned Fourier transforms of the simulated THz transmission were thus calculated. As shown in Fig. 3(b), the simulated spectra replicate the experimental results well, including the three distinct stages observed in our experiments.

Similar results were obtained in experimental studies of other polycrystalline samples, including nucleic acid bases, nucleosides, and mono- and disaccharides. Our experimental observations and theoretical simulations suggest that resonant absorption of a THz pulse followed by emission at the same frequency as the vibrational mode is a common feature of all Lorentz oscillators with resonance frequencies in the THz region. However, the experimental observation of far-IR/THz emission from a Lorentz oscillator is ultimately governed by the energy-time uncertainty, in which the time for measuring the oscillating electric field of far-IR emission cannot be longer than the lifetime of the oscillations.⁹ As a result, those oscillators with ultrashort lifetimes may never be detectable in the time domain, and may only appear as a broad feature in the frequency domain.

The THz technique reported here is also applicable to studies of gaseous samples. For example, far-IR emission has been reported for gaseous polycyclic aromatic hydrocarbons (PAHs), which may play an important role in the chemistry

of the interstellar medium.¹⁰ It has been hypothesized that PAH molecules absorb ultraviolet radiation, undergo internal conversion, and then emit radiation in the IR region. Therefore, time-domain THz absorption/emission spectroscopy may provide useful information in the assignment and explanation of unidentified spectral features from astronomical objects.

In summary, we have presented a time-resolved investigation of the resonant absorption of THz pulses and the subsequent vibrational relaxation processes in polycrystalline cytosine at 4 K. We found that the resonant absorption of a THz pulse is followed by the emission of THz radiation at the same frequency as the vibrational mode. We used a classical, Lorentz oscillator, model to simulate the damped oscillations of the electric field produced by excited molecules as they decay. The calculated results agree well with our experimental observations.

This work was supported by the Research Councils UK (Basic Technology Programme), Toshiba Research Europe Ltd. (EHL), and the Association of Commonwealth Universities (PCU).

¹C. C. Davies, in *Lasers and Electro-optics* (Cambridge University Press, Cambridge, UK, 1996), Chap. 1–2.

²B. R. Cohen and R. M. Hochstrasser, in *Infrared Spectroscopy of Biomolecules*, edited by H. Mantsch and D. Chapman (Wiley-Liss, New York, 1996), Chap. 5.

³M. Towrie, D. C. Grills, J. Dyer, J. A. Weinstein, P. Matousek, R. Barton, P. D. Bailey, N. Subramaniam, W. M. Kwok, C. Mia, D. Phillips, A. W. Parker, and M. W. George, *Appl. Spectrosc.* **57**, 367 (2003), and references therein.

⁴A. Xie, A. F. G. van der Meer, and R. H. Austin, *Phys. Rev. Lett.* **88**, 018102 (2002).

⁵M. C. Beard, G. M. Turner, and C. A. Schmuttenmaer, *J. Phys. Chem. B* **106**, 7146 (2002).

⁶Y. C. Shen, P. C. Upadhyaya, A. G. Davies, and E. H. Linfield, *Appl. Phys. Lett.* **82**, 2351 (2003).

⁷Q. Wu and X. C. Zhang, *Appl. Phys. Lett.* **67**, 3523 (1995).

⁸B. M. Fischer, M. Walther, and P. Uhd Jepsen, *Phys. Med. Biol.* **47**, 3807 (2002).

⁹M. Hase, M. Kitajima, A. M. Constantinescu, and H. Petek, *Nature (London)* **426**, 51 (2003).

¹⁰K. Zhang, B. Guo, P. Colarusso, and P. F. Bernath, *Science* **274**, 582 (1996).